Intracellular Monitoring Hot Paper

DOI: 10.1002/anie.201306390

Plasmonic Nanoprobes for Real-Time Optical Monitoring of Nitric Oxide inside Living Cells**

Pilar Rivera_Gil, Carmen Vazquez-Vazquez, Vincenzo Giannini, M. Pilar Callao, Wolfgang J. Parak, Miguel A. Correa-Duarte,* and Ramon A. Alvarez-Puebla**

The development of new methods (e.g. the use of remote sensors) to monitor biological processes inside living cells is essential to understand basic processes under pathophysiological circumstances, and consequently for the advancement of modern medicine. The use of remote optical sensors represents a powerful strategy, although their development faces several major problems related to the design of adequate active optical materials.[1] For example, limits exist regarding the selection of the chemoreceptors,[2] the biocompatibility,[3] interferences that result from the interaction of other biological species with the optical materials,[4] the prevention of sensor degradation under the experimental conditions,[5] multiplexing,[6] and the minimization of the sensor effect on the organism.[7] Here, we design plasmonic nanoprobes as advanced intracellular hybrid "all-optical" sensors for nitric oxide (NO). The sensors comprise a mesoporous silica coating with an inner gold island film functionalized with a chemoreceptor for NO. They enable the quantitative in situ real-time monitoring of the dynamics of NO in living cells (inside the lysosomes where the sensor particles are located)[8] without obvious impairment of the cells, even after days of experiments. Their sophisticated design prevents the interaction of lysosomal macromolecules with the active optical material and the enzymatic degradation of the sensor. Additionally, the sensors facilitate the diffusion of small molecules, such as NO, between their interior and exterior thanks to the plasmonic thermal gradients generated upon their illumination.

NO is an important physiological messenger and effector in mammalian cells. In fact, lysosomal functions are finely regulated by NO.[9] NO exhibits complex effects on the autophagy process, the degradation of the cell's own components to supply energy and nutrient for its growth,[10] and its effects are also closely related to various lysosomal disorders, such as Fabry, Gaucher, or Danon diseases.[11] A variety of NO-sensitive fluorescent molecular probes have been developed to image intracellular NO under one-[12] or two-photon microspectroscopy.[13] These methods, some of which are commercial (e.g. OxiSelect, Cell Biolabs; DAR-4M AM, Calbiochem; DAF-FM DA, Sigma Aldrich), have enhanced the understanding about NO homeostasis, but the probes are in general toxic, can degrade inside the lysosomes, or suffer from photobleaching upon repetitive illumination with light when monitoring for a long time. Conversely, the fact that these probes are fluorescent in the visible region implies potential cellular damage when excited for medium/long times.[14] Thus, to date, the real effect of NO in the lysosomes is not fully understood because of the lack of reliable methods to quantify the variations of NO levels in real time and in a dynamic range of concentrations.

Intracellular NO can be detected through its capacity to promote diazotization of certain aromatic amines.[15] Although the diazotization reaction is specific for NO, nitrogen oxides that generate NO under acidic conditions will also be detected. These include NO_2^-, which forms HNO_2 and NO, and any labile nitroso compound (R-NO) that can spontaneously release NO. The diazotization is 100 times more sensitive for NO and labile nitroso compounds than for NO_2^-. Nonetheless, the use of these chemoreceptors in surface-enhanced Raman scattering (SERS),[2] a powerful Raman-based ultrasensitive spectroscopy method, requires the appropriate plasmonic platform to provide the necessary electrical field for the Raman amplification.[16] In our case, we employed plasmonic capsules, in which the metallic particles

[*] Dr. P. Rivera_Gil,[+] Prof. W. J. Parak
Department of Physics, Philipps Universität Marburg
35037 Marburg (Germany)
E-mail: wolfgang.parak@physik.uni-marburg.de
C. Vazquez-Vazquez,[+] Prof. M. A. Correa-Duarte
Department of Physical Chemistry, University of Vigo
36310 Vigo (Spain)
E-mail: macorrea@uvigo.es
Dr. V. Giannini
Department of Physics, Imperial College London
London SW7 2AZ (UK)
Prof. M. P. Callao, Prof. R. A. Alvarez-Puebla
Department of Chemistry, Universitat Rovira i Virgili
43007 Tarragona (Spain)
Prof. R. A. Alvarez-Puebla
ICREA (Catalonian Institution for Research and Advanced Studies)
Avda. Lluís Companys, 08010 Barcelona (Spain)
and
Center for Chemical Technology of Catalonia
Edifici N5, Carrer de Marcel·lí Domingo, s/n 43007 Tarragona (Spain)
E-mail: ramon.alvarez@urv.cat
[+] These authors contributed equally to this work.

[**] This work was funded by the Spanish Ministerio de Economía y Competitividad (CTQ2011-23167), the European Research Council (CrossSERS, FP7/2013 329131, Metachem FP7/2008 228762-2), and the Human Frontier Science Program (grant RGP0052/2012-C201). We also acknowledge Niurka Llópiz Janer for her help with the cellular cultures.

Supporting information for this article is available on the WWW under http://dx.doi.org/10.1002/anie.201306390.

 © 2013 Wiley-VCH Verlag GmbH & Co. KGaA, Weinheim

that support the SERS chemoreceptor are protected with a mesoporous silica shell.[17] This shell allows the diffusion of the lysosomal solution from/to the particles and provides a stable, biocompatible, and heat-insulated support that inhibits the interaction of proteins, enzymes, and other macromolecules with the plasmonic surfaces.

The capsules were prepared by deposition of gold nanoparticles onto polymer beads, coating with mesoporous silica, and calcination to remove the organic polymer. The presence of the gold particles in the interior allows their epitaxial growth under mild conditions (see the Supporting Information). Figure 1a and Figure S1 (in the Supporting Information) show scanning electron microscopy (SEM) images of the materials under different magnifications. The slicing of a capsule with a focused ion beam permits the observation of the hollow nature of the material where the gold nanoparticles (40 nm) are attached to the interior silica walls. Furthermore, scanning transmission electron microscopy (STEM) and X-ray energy dispersive spectroscopy (XEDS; Figure 1b) provide evidence of the epitaxial growth of gold nanoparticles in the inner space of the silica capsule, as no trace of gold was detected on the outer surface. Notably, after the growth of gold nanoparticles, the localized surface plasmon resonance of the capsules shifts to the red region and broadens (Figure S2a). This result provides evidence of the coupling of the electromagnetic fields of different particles, thus providing the so-called hot spots.[18] The localization of these highly active optical regions was simulated with numerical methods on a cross section of the capsule (Figure S2b). The efficiency was confirmed by SERS spectroscopy (Figure S2c) of *p*-aminobenzenethiol (ABT).[19]

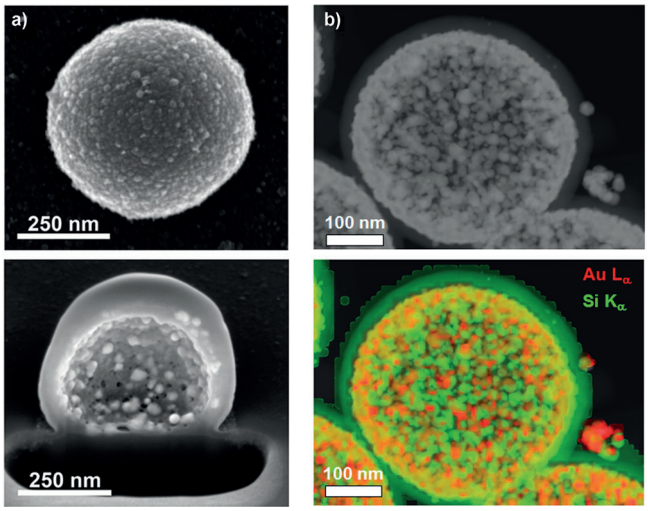

Figure 1. a) SEM image and cross-sectional image of the interior of a hollow mesoporous silica capsule with inner gold nanoparticles. b) STEM and XEDS mappings showing elemental distribution of gold (red) and silica (green).

To form the sensor, the gold particles inside the capsules were capped with ABT. This molecule was selected because of the thiol group, which can covalently bind to gold, and the amino group, which can diazotize with an equimolecular concentration of NO at an acidic pH value. Notably, our plasmonic capsules provide an electromagnetic field upon illumination, and the intense optical absorption at the surface plasmon resonance frequency is responsible for a strong heat generation through an efficient photo-heat conversion.[20] The numerical solution of the Poisson equation gives us an estimation of the temperature inside the capsule upon illumination with NIR light (785 nm; Figure S3).[21] This theoretical simulation of the thermal properties shows that while the temperature of the aqueous solution in the interior of the capsule is rising to 90 °C, the conductive heat transfer to the lysosomal solution is completely hindered by the highly insulating silica shell, thus avoiding damages in the cell.[22] The generation of heat has three important consequences. First, this heat generates a thermal gradient with the subsequent convective current in between the interior and the exterior of the capsule making the diffusion of NO considerably faster. Second, as the temperature increases, the rate of diazotization increases, thus decreasing the amount of protons necessary to give the diazonium salt. Third, the diazonium salt is only stable at low temperatures and spontaneously degrades to an alcohol and a nitrogen molecule through the reaction with water (Figure S4).[23] This reaction can be exploited for the quantitative determination with SERS. Figure 2a shows the initial spectra of ABT before and after the exposure to variable concentrations of NO. Notably, the characteristic ring stretching of ABT at 1548 cm^{-1} and the in-plane C-N-H deformation at 1604 cm^{-1} disappear, while bands at 1583 and 1529 cm^{-1}, ascribed to the ring stretching and the in-plane C-O-H deformation of hydroxybenzenethiol[24] (HBT) appear, which is due to the transformation of ABT to HBT (Figure 2b). This chemical transformation allows the monitoring of NO by correlating the relative intensity of the two ring stretching bands (1548 and 1583 cm^{-1} from ABT and HBT, respectively) as $I_{1583}/(I_{1583}+I_{1548})$. To do so, the areas under the bands at 1548 and 1583 cm^{-1} were deconvoluted, assuming a Lorentzian shape, where the band position and the full widths at half maxima are fixed (Figure 2b). To test the efficiency of our capsules under biological conditions, an experiment was designed by employing the surface response methodology[25] and varying both ionic strength (0–0.2 M in NaCl) and pH value (4–6.5) in the growth medium (Dulbecco's modified Eagle's medium (DMEM) supplemented with 10% fetal bovine serum (FBS), 1% L-glutamin, and 1% penicillin/streptomycin (% in weight). The obtained response surface (Figure 2c) shows that even though the ionic strength has no impact on the measurement, the pH value is essential. Diazotization inside the capsules can only be considered quantitatively at pH values below five. This observation is important, because while the common pH value inside the cytosol is 7.4, the lysosomal fluid (where the capsules incorporated by cells reside) is acidic, with values below pH 4. When applying the deconvolution process to solutions that contain different concentrations of NO at a fixed pH value (4.5) and ionic strength (0.1 M), and plotting the band intensity ratio $I_{1583}/(I_{1583}+I_{1548})$ against the concentration of NO, the result is a linear correlation with an impressive correlation coefficient (r^2) value of 0.981 (Figure 2d), thus demonstrating the quantitative nature of this analytical

 © 2013 Wiley-VCH Verlag GmbH & Co. KGaA, Weinheim

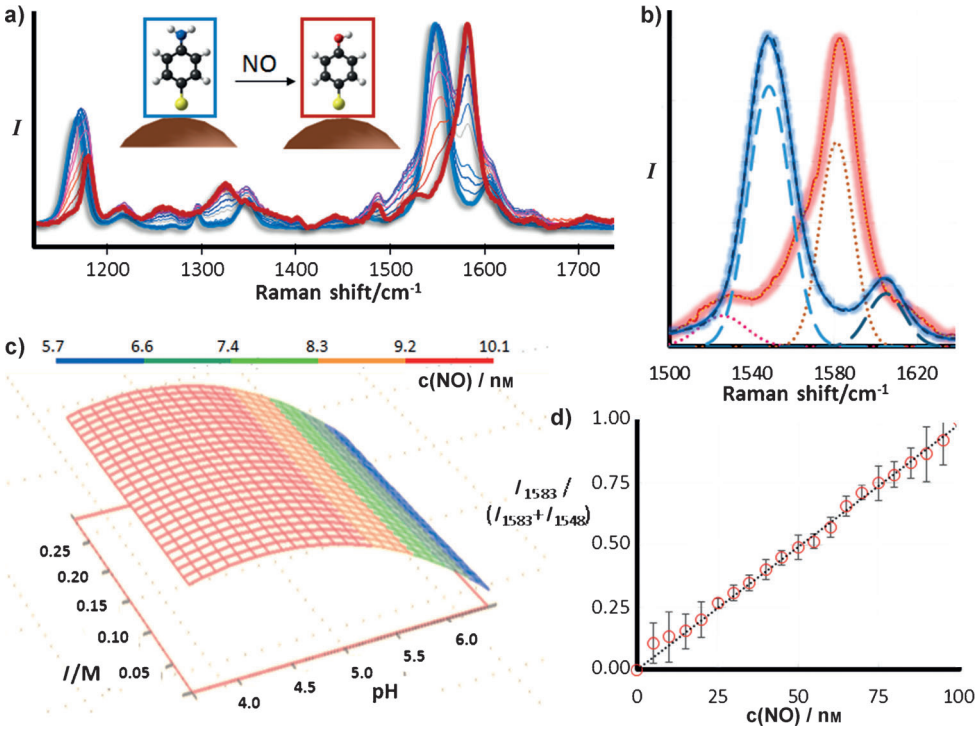

Figure 2. a) SERS spectra of the capsules as a function of NO concentration. Spectra of ABT (blue) and HBT (red) are shown for comparison. Thin traces in between represent the resulting spectra with growing concentrations of NO. b) Results for the deconvolution of the characteristic ring stretching bands for ABT (blue) and HBT (red). The highlighted traces represent the experimental spectra, the dashed and dotted spectra beneath them are the result of co-adding the deconvoluted peaks (unhighlighted dashed and dotted traces). c) Response surface plot for the determination of NO (10 nM experimentally added) in biological media at a variable pH value (4–6) and ionic strength (I) in NaCl (0–0.25 M). d) Linear plot of the ABT (1548 cm^{-1}) and (HBT 1583 cm^{-1}) ring stretching intensity ratios ($I_{1583}/(I_{1583}+I_{1548})$) as a function of the NO concentration (pH 4.5, $I=0.1$ M). Error bars represent the standard deviations in five replicated experiments.

method. However, the capsules become less sensitive at low concentrations, as the changes in the ABT spectra upon reaction with NO become less pronounced. Nevertheless, the capsules offer a good estimation of the NO levels that are present, which can be clearly observed in the surface response experiment, where the level of NO (experimentally 10 nM) fluctuates by less than 8% under the biological conditions found in the lysosome (Figure 2c).

As a first experiment for intracellular monitoring of lysosomal NO, we used 3T3 embryonic fibroblasts. Figures 3 and S5 show that the capsules (reflected light is shown in green) are effectively internalized by the cells. The white arrow shows an example of several capsules attached to extracellular sites of the cells (cytoskeleton stained in red). The internalized capsules localized as expected within lysosomes (yellow).[8] Next, the same protocol was followed with unlabeled cells and capsules (Figure S6). Contrary to other sensors,[13] our sensor turned out to be highly viable and compatible with the cells. Even in the presence of capsules, 97% of cells were viable (see the Supporting Information). For SERS monitoring, although capsules were visible under a confocal microscope with a 100× objective, a wide area was mapped with a NIR laser. Notably, the SERS spectra in the different regions (highlighted in Figure 4a with green and orange dotted circles) showed small concentrations of NO between 5 and 10 nM under normal conditions. These results contrast with those of extracellular capsules (black or pink dotted circles) or the capsules in the media without cells, both showing the bare spectra of ABT (Figure S7). Also, for comparison, cells mapped under the same conditions, but without capsules, showed no signal (Figure S8). As a final step, we conducted the same experiment, but induced the generation of NO by adding hydrogen peroxide (H_2O_2).[26] In this case, we monitored the same capsule over time in three different experiments. Figure 4b shows the measurements obtained in three different experiments. The three curves show a linear growth to reach a plateau 4 h after the addition. In contrast, the same control experiments, without the addition of H_2O_2, show stable levels of NO (Figure 4b and Figure S9), thus demonstrating the ability of the sensor to

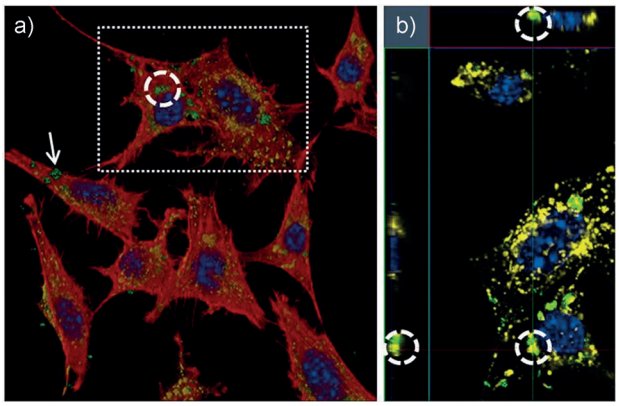

Figure 3. Intracellular localization of the capsules in stained 3T3 cells (NO sensors: green; lysosomes: yellow; cytoskeleton: red; and nucleus: blue). The capsules are effectively internalized by the cells and localize within lysosomes, as observed by the co-localization of the signal intensity of the different dyes and the reflected light of the sensor. a) Corresponds to a 3D reconstruction of the Z-scan of a cell area. b) A selected area (dashed line) was observed in the different planes (X/Y; X/Z; Y/Z). For a better recognition of intralysosomal localization of the sensors, only the sensor, the lysosome, and the nucleus are shown.

© 2013 Wiley-VCH Verlag GmbH & Co. KGaA, Weinheim

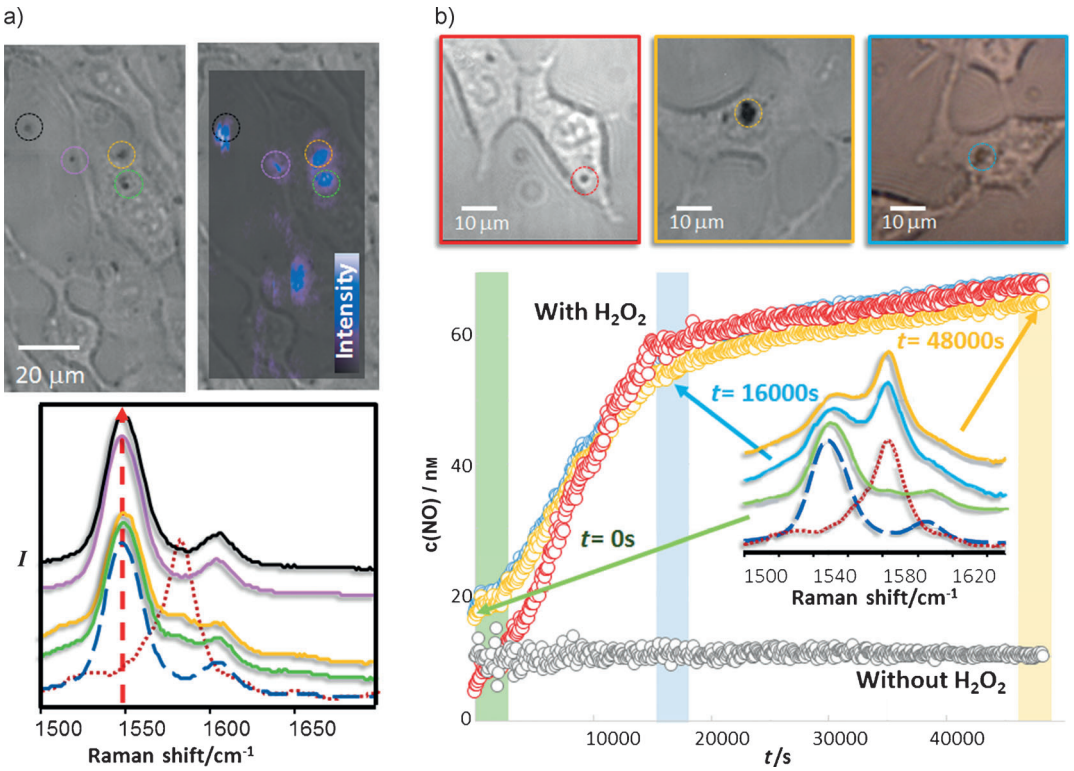

Figure 4. a) Optical and SERS (mapped at 1548 cm^{-1}, as marked with the arrow below) images of 3T3 cells in the presence of capsules. The SERS spectra (bottom) show the signals for the colored circles in the image (top). b) Optical images and intracellular NO formation over time (obtained through the $I_{1583}/(I_{1583}+I_{1548})$ relation) for three different samples upon NO induction with oxygen peroxide (H_2O_2). A control sample without the presence of H_2O_2 is also shown for comparison. Representative normalized SERS spectra obtained at different times are shown. The SERS dashed (blue) and dotted (red) spectra represent the reference vibrational pattern for ABT and HBT, respectively.

detect the dynamic concentration of intracellular (intralysosomal) NO in a basically non-invasive way.

In conclusion, our approach is an important step forward in the development of intracellular sensors for the quantitative detection of small analytes. Please note that in general, particle-based cellular (in vitro) sensing has the advantage that (hours after incubation) the biodistribution of the sensor remains constant (in the lysosome), whereas molecular sensors are typically not clearly localized to a particular cellular compartment over extended periods of time.[27] This sensing method has also the advantages of an improved biocompatibility, and a better signal-to-noise ratio because of the increased concentration of plasmonic material per sensing particle.[28] Intracellular particle-based fluorescence sensing of different analytes has been reported,[27,29] but is associated with several experimental complications. Many analyte-sensitive fluorophores (e.g. for K^+ or Na^+) are extremely affected by pH,[6] which makes a quantitative detection complicated. Multiplexed read-out of several fluorophores in parallel is complicated by the relatively large spectral width of their emission spectra, which can only be circumvented by tricks, such as barcoding of spatially resolved individual sensor particles.[6] In addition, fluorophores tend to photobleach, which also makes quantitative intracellular detection of analytes over extended periods of time complicated.[30] In our case, the detection signal is based on SERS, which is more stable in time compared to fluorescence read-out. Second, in our case, an acidic pH value results in the detection of NO and excludes crosstalk with sensors that have not been internalized by cells. Also, multiplexed detection can be envisaged, as the sharp bands of SERS emission signals originating from different analyte-sensitive molecules can be spectrally resolved.[31] SERS detection of analytes, in particular the pH value, has been reported before on the level of single plasmonic nanoparticles.[32] However, SERS read-out based on individual nanoparticles suffers from particle agglomeration,[33] and this favors the creation of new hot spots and thus changes in signal intensity. Upon internalization of nanoparticles, they ultimately get closely packed inside endosomes/lysosomes, so that the read-out of such a system is not stable over time and is thus not suited well for quantitative localized sensing. In contrast, the particle geometry we employed elegantly circumvents this problem by assembling the plasmonic nanoparticles in a fixed geometry in the silica shell of a bigger particle. Thus their distance remains constant, even upon cellular uptake, and the SERS signal is stable over time. Therefore, the sensors developed here have the future capacity to reside inside cells as intracellular reporters for multiplexed on-line detection of multiple analytes.

Received: July 22, 2013
Revised: September 5, 2013
Published online: November 12, 2013

 © 2013 Wiley-VCH Verlag GmbH & Co. KGaA, Weinheim

Keywords: analytical methods · intracellular monitoring · nanostructures · nitrogen oxides · optical sensors

[1] a) A. Z. Abbasi, F. Amin, T. Niebling, S. Friede, M. Ochs, S. Carregal-Romero, J.-M. Montenegro, P. Rivera Gil, W. Heimbrodt, W. J. Parak, *ACS Nano* **2011**, *5*, 21 – 25; b) S. Carregal-Romero, J.-M. Montenegro, W. J. Parak, P. Rivera Gil, *Front. Pharmacol.* **2012**, *3*, 70 – 76.
[2] R. A. Alvarez-Puebla, L. M. Liz-Marzán, *Angew. Chem.* **2012**, *124*, 11376 – 11385; *Angew. Chem. Int. Ed.* **2012**, *51*, 11214 – 11223.
[3] a) F. Tang, L. Li, D. Chen, *Adv. Mater.* **2012**, *24*, 1504 – 1534; b) D. Tarn, C. E. Ashley, M. Xue, E. C. Carnes, J. I. Zink, C. J. Brinker, *Acc. Chem. Res.* **2013**, *46*, 792 – 801.
[4] J. Klein, *Proc. Natl. Acad. Sci. USA* **2007**, *104*, 2029 – 2030.
[5] J. Vogelsang, R. Kasper, C. Steinhauer, B. Person, M. Heilemann, M. Sauer, P. Tinnefeld, *Angew. Chem.* **2008**, *120*, 5545 – 5550; *Angew. Chem. Int. Ed.* **2008**, *47*, 5465 – 5469.
[6] L. L. del Mercato, A. Z. Abbasi, M. Ochs, W. J. Parak, *ACS Nano* **2011**, *5*, 9668 – 9674.
[7] a) P. Rivera-Gil, D. Jimenez De Aberasturi, V. Wulf, B. Pelaz, P. Del Pino, Y. Zhao, J. M. De La Fuente, I. Ruiz De Larramendi, T. Rojo, X. J. Liang, W. J. Parak, *Acc. Chem. Res.* **2013**, *46*, 743 – 749; b) R. Bardhan, S. Lal, A. Joshi, N. J. Halas, *Acc. Chem. Res.* **2011**, *44*, 936 – 946.
[8] L. Kastl, D. Sasse, V. Wulf, R. Hartmann, J. Mircheski, C. Ranke, S. Carregal-Romero, J. A. Martínez-López, R. Fernández-Chacón, W. J. Parak, H.-P. Elsasser, P. Rivera_Gil, *ACS Nano* **2013**, *7*, 6605 – 6618.
[9] T. Shintani, D. J. Klionsky, *Science* **2004**, *306*, 990 – 995.
[10] J. D. Rabinowitz, E. White, *Science* **2010**, *330*, 1344 – 1348.
[11] L. J. Ignarro, *Nitric Oxide: Biology and Pathobiology*, Academic Press, New York, **2000**.
[12] M. H. Lim, D. Xu, S. J. Lippard, *Nat. Chem. Biol.* **2006**, *2*, 375 – 380.
[13] H. Yu, Y. Xiao, L. Jin, *J. Am. Chem. Soc.* **2012**, *134*, 17486 – 17489.
[14] G. J. Puppels, J. H. F. Olminkhof, G. M. J. Segers-Nolten, C. Otto, F. F. M. de Mul, J. Greve, *Exp. Cell Res.* **1991**, *195*, 361 – 367.
[15] a) Y. Yang, S. K. Seidlits, M. M. Adams, V. M. Lynch, C. E. Schmidt, E. V. Anslyn, J. B. Shear, *J. Am. Chem. Soc.* **2010**, *132*, 13114 – 13116; b) L. J. Ignarro, G. M. Buga, K. S. Wood, R. E. Byrns, G. Chaudhuri, *Proc. Natl. Acad. Sci. USA* **1987**, *84*, 9265 – 9269.
[16] P. L. Stiles, J. A. Dieringer, N. C. Shah, R. P. Van Duyne, *Annu. Rev. Anal. Chem.* **2008**, *1*, 601 – 626.
[17] a) M. Sanlés-Sobrido, M. Pérez-Lorenzo, B. Rodríguez-González, V. Salgueiriño, M. A. Correa-Duarte, *Angew. Chem.* **2012**, *124*, 3943 – 3948; *Angew. Chem. Int. Ed.* **2012**, *51*, 3877 – 3882; b) M. Sanles-Sobrido, W. Exner, L. Rodriguez-Lorenzo, B. Rodriguez-Gonzalez, M. A. Correa-Duarte, R. A. Alvarez-Puebla, L. M. Liz-Marzan, *J. Am. Chem. Soc.* **2009**, *131*, 2699 – 2705.
[18] D.-K. Lim, K.-S. Jeon, J.-H. Hwang, H. Kim, S. Kwon, Y. D. Suh, J.-M. Nam, *Nat. Nanotechnol.* **2011**, *6*, 452 – 460.
[19] M. Sun, Y. Huang, L. Xia, X. Chen, H. Xu, *J. Phys. Chem. C* **2011**, *115*, 9629 – 9636.
[20] J. R. Adleman, D. A. Boyd, D. G. Goodwin, D. Psaltis, *Nano Lett.* **2009**, *9*, 4417 – 4423.
[21] a) G. Baffou, C. Girard, R. Quidant, *Phys. Rev. Lett.* **2010**, *104*, 136805; b) C. Vázquez-Vázquez, B. Vaz, V. Giannini, M. Pérez-Lorenzo, R. A. Alvarez-Puebla, M. A. Correa-Duarte, *J. Am. Chem. Soc.* **2013**, *135*, 13616 – 13619.
[22] Q. Yue, Y. Li, M. Kong, J. Huang, X. Zhao, J. Liu, R. E. Williford, *J. Mater. Chem.* **2011**, *21*, 12041 – 12046.
[23] C. E. Waring, J. R. Abrams, *J. Am. Chem. Soc.* **1941**, *63*, 2757 – 2762.
[24] W. Ji, X. Xue, W. Ruan, C. Wang, N. Ji, L. Chen, Z. Li, W. Song, B. Zhao, J. R. Lombardi, *Chem. Commun.* **2011**, *47*, 2426 – 2428.
[25] R. H. Myers, D. C. Montgomery, C. M. Anderson-Cook, *Response Surface Methodology: Process and Product Optimization Using Designed Experiments*, Wiley, Hoboken, **2009**.
[26] S. R. Thomas, K. Chen, J. F. Keaney, *J. Biol. Chem.* **2002**, *277*, 6017 – 6024.
[27] P. Rivera-Gil, M. Nazarenus, S. Ashraf, W. J. Parak, *Small* **2012**, *8*, 943 – 948.
[28] P. Rivera Gil, L. L. Del Mercato, P. del_Pino, A. Muñoz_Javier, W. J. Parak, *Nano Today* **2008**, *3*, 12 – 21.
[29] S. M. Buck, H. Xu, M. Brasuel, M. A. Philbert, R. Kopelman, *Talanta* **2004**, *63*, 41 – 59.
[30] O. Kreft, A. M. Javier, G. B. Sukhorukov, W. J. Parak, *J. Mater. Chem.* **2007**, *17*, 4471 – 4476.
[31] L. Rodriguez-Lorenzo, L. Fabris, R. A. Alvarez-Puebla, *Anal. Chim. Acta* **2012**, *745*, 10 – 23.
[32] J. Kneipp, H. Kneipp, B. Wittig, K. Kneipp, *J. Phys. Chem. C* **2010**, *114*, 7421 – 7426.
[33] J. Kneipp, H. Kneipp, M. McLaughlin, D. Brown, K. Kneipp, *Nano Lett.* **2006**, *6*, 2225 – 2231.

 © 2013 Wiley-VCH Verlag GmbH & Co. KGaA, Weinheim